Phase Field Modelling of Microstructural Changes in NI/YSZ Solid Oxide Electrolysis Cell Electrodes

Trini, M.; De Angelis, S.; Jørgensen, P. S.; Hauch, A.; Chen, M.; Hendriksen, P. V.

Published in:
Proceeding of the 42nd International Conference on Advanced Ceramics and Composites

Link to article, DOI:
10.1002/9781119543343.ch16

Publication date:
2019

Document Version
Peer reviewed version

PHASE FIELD MODELLING OF MICROSTRUCTURAL CHANGES IN NI/YSZ SOLID OXIDE ELECTROLYSIS CELL ELECTRODES

M. Trini, S. De Angelis, P. S. Jørgensen, A. Hauch, M. Chen and P. V. Hendriksen
Department of Energy Conversion and Storage, Technical University of Denmark
Roskilde, Denmark

ABSTRACT

Solid oxide cells (SOC) are electrochemical devices that can operate efficiently both in fuel cell (solid oxide fuel cell, SOFC) and electrolysis mode (solid oxide electrolysis cell, SOEC). However, long-term performance degradation hinder the widespread commercialization of this technology. Nickel coarsening is a major cause of the decrease of the cells' performance. Therefore, investigating and quantifying effects of nickel coarsening on the microstructural evolution in SOCs is crucial to understand the degradation processes occurring during operation.

Focused-ion-beam scanning electron microscopy (FIB-SEM) tomography and phase field (PF) modelling are used to investigate the microstructure evolution of Ni/Yttria-Stabilized Zirconia (YSZ) SOC fuel electrodes.

A cell, tested as part of a 25 cells stack for 9000 hours, and a reference cell (never operated) are reconstructed using FIB-SEM tomography. Microstructural parameters were calculated on the two cells showing that the percolated triple phase boundary (TPB) length in the cell decreases from 1.85 $\mu m/\mu m^3$ for the reference cell to only 1.01 $\mu m/\mu m^3$ for the long-term tested one.

Phase field simulations were run on the reference cell geometry and microstructural parameters such as particle size distribution (PSD), TPB length and surface areas are computed and quantified on the simulated volumes. A trend of decreasing percolated TPB length with time is observed in the simulations. The numerical results are used to investigate the effects of nickel coarsening as well as to obtain information on the kinetics of the phenomenon.

INTRODUCTION

SOCs may play a key role in the future energy scenario, where renewable intermittent sources will be extensively and increasingly used for electricity production. The possibility of operating SOCs in fuel cell (SOFC) and electrolysis (SOEC) mode makes it possible to use SOC as electrochemical devices that can store energy in chemical form. Electrical energy from overproduction can be stored as fuel and then converted to electricity when needed. In this regard, cost, efficiency, and durability of the conversion devices will be of key importance for the market penetration of the technology.

At least five years of operation are required for the market breakthrough of such devices [1, 2]. Therefore, long-term microstructural degradation still represents a critical issue for the SOC technology. A deep understanding of the processes occurring at the micro- and nano-scale and a proper characterization of the structure are essential to optimize performance.

Among several long-term degradation processes previously reported[3, 4, 5, 6, 7, 8,] nickel coarsening in the Ni/YSZ (Yttria-Stabilized Zirconia) cermet is considered to be one of the main causes of long-term cell degradation[4, 9, 10, 11]. The coarsening process is driven by the transport of Ni atoms from regions with high curvature towards regions with low curvature, in order to minimize the system free energy according to the Gibbs-Thomson effect[12]. It has been observed that the Ni coarsening substantially affects the electrode microstructure in the first thousand hours of cell operation[13].

The cell operating conditions (e.g. temperature, gas composition, current density) strongly influence the changes in the electrode microstructure. Nickel tends to detach from the

YSZ structure and reorganize into bigger and more rounded particles[14]. This effect leads to a shift in continuous particle size distribution towards bigger particles radii and to the loss of active TPB sites[15].

Predicting the evolution of the electrode microstructure after long-term operation through numerical modelling is important. A deep understanding of nickel coarsening causes can allow optimization of production processes and/or operation schemes, guiding the development of engineered microstructures less prone to degradation. Several models have been developed to study the Ni coarsening; Vaßen et al.[13] used a two particles approach based on Fick´s law for vacancy diffusion to simulate the Ni particles agglomeration in Ni/YSZ SOC electrodes. A refined two particles model was implemented by Gao et al.[16] while Kennouche et al.[17] adopted a power law model to predict the average particle size after 100000 hours. However, these simplified models cannot predict the evolution of a complex Ni/YSZ microstructure. Recently, three-dimensional PF models, able to simulate Ni coarsening in a real 3D microstructure, have been used to predict the evolution of Ni/YSZ electrodes[12, 18, 19].

Phase field modelling has been extensively used to model mesoscale changes in the microstructure of complex structures[20], describing the material boundaries through a finite thickness diffuse interface. In a multi-phase system, each phase can be described by a phase variable, the order parameter (OP). Each OP assumes two constant values inside and outside the phase of interest varying smoothly across the interfaces of the phases. All the interface information are included in the OPs, while immiscibility and interfacial energies are incorporated in the model through the bulk free energy and the gradient energy penalty, respectively.

In this paper, we performed focused ion beam scanning electron microscopy (FIB-SEM) tomography on two SOEC: a reference cell not tested, and a cell tested for approximately 9000 hours. Long-term microstructural degradation was characterized by means of microstructural parameters computed on the experimental datasets. Finally, in order to investigate the earlier stages of Ni coarsening, phase field simulations were run using the reconstructed reference geometry as input parameters for the model. Preliminary results of the phase-field simulations are presented here. (Further work to validate the model is ongoing).

EXPERIMENTAL

In this work, we analyzed a SOC tested in electrolysis mode as part of a stack for approximately 9000 hours. Preliminary 1D and 3D characterizations of the same cell were performed on different sample locations and have been reported in Ref.[15]. The stack was composed by 25 cells with Ni/YSZ support layer and fuel electrode, a YSZ electrolyte, and a LSFC-CGO (LSFC: $(La,Sr)(Co,Fe)O_{3-\delta}$, CGO: $(Ce,Gd)O_2$) oxygen electrode and a CGO barrier layer. The electrochemical tests were carried out at the European Institute for Energy Research. The stack was tested for 2175 hours at a current density of -0.57 A/cm^2 which was then, increased to -0.72 A/cm^2 for the following 4785 hours of the test[21]. The average temperature and steam conversion of the stack were kept constant at 750 °C and 50%, respectively. The steam/hydrogen ratio at the inlet side was 90/10. More details on the electrochemical tests and stack performance can be found in[21].

After 9000 hours of operation, the stack was embedded in epoxy resin. A Zeiss XB1540 Crossbeam field emission gun SEM was used for data acquisition on a reference cell (i.e. a cell from the same cell production batch reduced at 1000°C for 2 hours in 9 % H_2 in N_2 with ~ 4 % of steam and not tested further) and on the inlet side of the tested cell. The two data sets were obtained with slightly different microscope set-up, leading to different voxel sizes: 25 x 25 x 39.5 nm^3 for the reference and 25 x 25 x 35.6 nm^3 for the inlet-tested-cell data set. Volumes of ~ 12.5 x 8 x 20 µm^3 were obtained from FIB-SEM tomography for both reference and long-term tested

cell. However, in order to reduce the computational cost for the phase field simulation, sub-volumes of approximately 7.5 x 7.5 x 10.7 μm^3, were extracted from the original datasets.

We focused our study on the innermost part of the active fuel electrode by considering only the fuel electrode ~ 1μm from the electrode-electrolyte interface ending ~ 1μm from the interface between the active electrode and the support layer. The FIB-milling was perpendicular to the electrode-electrolyte interface as explained in[22]. Phase fractions, continuous PSD[23] and, total and percolating TPB length were computed on the experimental fuel electrode volumes as in[22].

To estimate the statistical accuracy of the calculated microstructural parameters, the analysis was performed on the entire FIB-SEM data set acquired for the reference cell. The error of each parameter was then evaluated as the relative change between the results obtained from the original volume and the extracted sub-volume.

The sub-volume extracted from the reference cell was used as input for phase field simulations. Microstructural parameters, (i.e. phase fractions, continuous PSD and TPB) were computed on the simulated volumes every 500000 iterations.

PHASE FIELD MODEL FORMULATION

The following assumptions were made in order to simplify the model:

1. At the operating temperature of a typical SOC, Ni evaporation can be considered negligible[24] and the volume (mass) of all the phases in the electrode is assumed conserved. Therefore, we used the Chan-Hilliard (conserved) equation to describe the dynamic of the system.
2. Based on previous experimental characterizations of the same sample[15], we assume that changes in the electrode are controlled by Ni evolution in a stationary YSZ matrix. Thus, the system can be described by only one OP, which evolves during the simulation.
3. The nickel surface tension is considered independent of crystal orientation[25].
4. The dominant transport mechanism that leads to the Ni coarsening is the Ni surface diffusion[12].

The Chan-Hilliard equation for one OP C, is expressed as follow

$$\frac{\partial C}{\partial t} = \nabla \cdot M \nabla \mu \tag{1}$$

where M is the mobility function and μ is the chemical potential. The chemical potential μ is defined as the functional derivative of the free energy functional F with respect to C:

$$\mu = \frac{\delta F}{\delta C} = \frac{\partial f}{\partial C} - \varepsilon^2 \nabla^2 C \tag{2}$$

The energy functional F is given by $F = \int_V \left[\frac{\varepsilon^2}{2}|\nabla C|^2 + f(C)\right] dV$ where ε is the gradient energy coefficient. The energy density is expressed by a double well potential function $f(C) = \frac{Q}{4} C^2 (1 - C)^2$ where Q is the height reached by the potential between the two minimum free energy states. ε and Q are linked to the interface width δ through the relation $\delta = \varepsilon\sqrt{2/Q}$ [26].

In this study, we used the Smoothed Boundary Method (SBM)[27] to implement the no-flux boundary conditions (BC) at the YSZ interface, and the contact angle BC at the triple junctions, as explained in [12]. In the SBM, a domain parameter ψ is introduced to identify the boundaries of the simulation domain. In this work, ψ assumes values ranging from 0 (inside the YSZ) to 1 (elsewhere), varying smoothly at the interfaces. The unit normal to the YSZ interface is defined as $\boldsymbol{n} = \nabla\psi/|\nabla\psi|$ while the contact angle θ between Ni and YSZ at the TPB can be

expressed in terms of ψ and C as $(\nabla\psi/|\nabla\psi|)\cdot(\nabla C/|\nabla C|) = -cos\theta$. Using the planar solution of the Young equation, we can deduce the SBM contact-angle BC as:

$$\nabla\psi\cdot\nabla C = -|\nabla\psi|\, cos\theta\, \frac{\sqrt{2f}}{\varepsilon} \tag{3}$$

The phase field governing equation with no-flux and contact angle BC, derived from the SBM formulation is:

$$\frac{\partial(\psi C)}{\partial t} = \nabla\cdot\left\{\psi M\nabla\left[\frac{df}{dC} - \frac{\varepsilon^2}{\psi}\left(\nabla\cdot(\psi\nabla C) + \frac{|\nabla\psi|\sqrt{2f}}{\varepsilon}cos\theta\right)\right]\right\} \tag{4}$$

In our model, to simulate only surface diffusion, we used the mobility function proposed by Chen et al. in[12], where M is a function of the order parameter C and the domain parameter ψ :

$$M(C,\psi) = M_{Ni-Pore}C^2(1-C)^2 g(\psi) \tag{5}$$

The function $g(\psi) = \psi^6(10\psi^2 - 15\psi + 6)$ is used to regulate the mobility close to the TPB [12, 28]. In this work, we used the central-difference method for the spatial discretization and the explicit forward-Euler scheme for the time discretization. The solver is implemented in C++ and parallelized using the Message Parsing Interface (MPI) library. All the simulations were run on 64 processors for a total computing time of ~ 216 hours.

Following Davis et al. in[29], a characteristic time τ is introduced to link the dimensionless time (used in the simulations) to the real time. The characteristic time can be expressed as:

$$\tau = \frac{L_0^4\left(\partial^2 f/\partial C^2\right)_{C_{eq}}}{ED_s\delta_s^2} \simeq \frac{16W_C^2L_0^4}{D_s\delta_s^2} \tag{6}$$

where L_0 is a characteristic length (voxel size, 25 nm), E is a reference energy density, D_s the surface self-diffusion, δ_s the interface width and W_C^2 is expressed by $W_C^2 = Q/(2E)$. The characteristic time obtained with the parameters in Table 1 is 1.206 s.

Table 1. Parameters used for calculating the characteristic time τ

L_0	W_C^2	D_s	δ_s
25 nm	1.93 m^{-1} [26]	10^{-11} m^2s^{-1} [26]	1 nm [26]

In this work, 10^7 iterations (corresponding to approximately 183 hours of operation) were run using the experimentally reconstructed reference cell microstructure as the initial condition. The sharp interfaces of the YSZ and Ni phases, obtained from the segmented data, are made diffuse by constructing two signed distance functions and fitting them to hyperbolic tangent functions[27]. The domain interface width must be as small as possible, in order to limit numerical errors, although big enough to ensure numerical stability. An interface of five grid points, corresponding to 125 nm, has been used in this study.

The segmentation of the simulated volumes was performed using the order parameter C and the domain parameter ψ. Regions where $C > 0.5$ and $\psi > 0.5$ are labeled as Ni phase, the YSZ is assigned where $\psi < 0.5$ and the remaining part of the domain ($C < 0.5$ and $\psi > 0.5$) is

attributed to the pores. The same statistical analysis mentioned in the Experimental section was performed on the simulation outputs.

RESULTS

Experimental

Figure 1a) and b) shows the two volumes analyzed for the reference cell and the cell that had operated for 9000 hours, respectively. Figure 1c) shows the corresponding Ni particle size distributions. It is possible to observe a shift of the particles radii towards larger values for the long-term tested cell piece. Approximately 50 % of the Ni particles in the reference cell consists of particles with a radius of ~ 400 nm or less, this value shifted to ~ 600 nm for the tested cell.

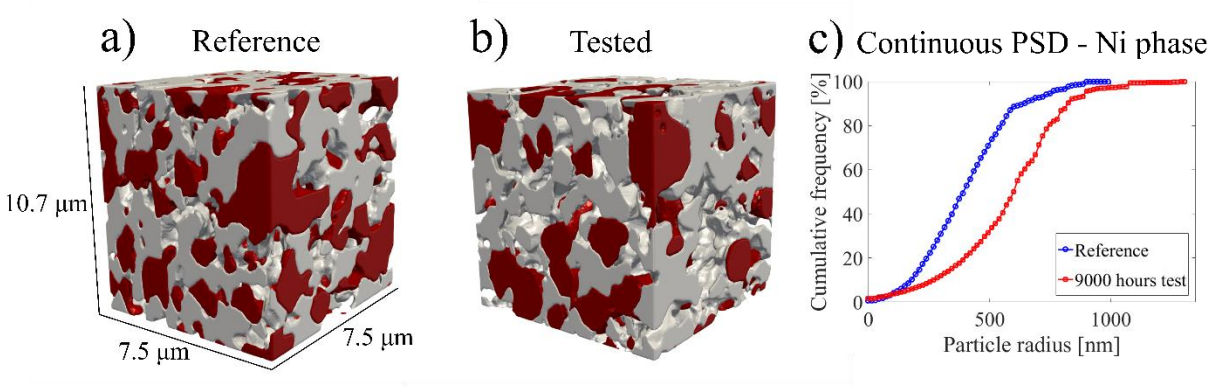

Figure 1. a) 3D rendering of the reference cell microstructure. b) 3D rendering of the tested cell microstructure. c) Cumulative continuous PSD of nickel for the reference (blue) and tested cell (red). In a) and b), nickel is shown in red, the YSZ in gray and the pores are transparent

The quantification of microstructural parameters computed on these volumes is summarized in Table 2. Changes in the phase fractions of the three phases were observed: approximately 14 % of Ni was lost in the innermost active fuel electrode after the long-term test. Consequently, the porosity in the region analyzed increased.

A decrease in total and percolating TPB length was observed after the long-term test. In particular, starting from 1.85 µm/µm^3 of percolated TPBs in the reference cell, only 1.01 µm/µm^3 were still present in the aged sample, which in turn means a decrease in electrochemical active sites in the long-term tested electrode. Finally, the overall Ni surface area and the interface area between Ni and YSZ and Ni and pore showed a reduction after the long-term test.

Table 2. Microstructural parameters computed on the reference, tested and simulated 3D geometries after 10^7 iterations corresponding to a characteristic time of app. 183 h.

	Reference	9000 hours tested cell	Simulated (10^7 iterations)
Ni [%]	29	25	29
YSZ [%]	45	43	45
Pore [%]	26	32	26

Total TPB [µm/µm^3]	2.38	1.55	1.87
Percolating TPB [µm/µm^3]	1.85	1.01	1.40
Pore surface area[µm^2/µm^3]	1.69	1.76	1.67
YSZ surface area [µm^2/µm^3]	1.96	2.02	1.96
Ni surface area [µm^2/µm^3]	1.44	0.91	1.29
Pore/YSZ interface area [µm^2/µm^3]	1.10	1.43	1.17
Pore/Ni interface area [µm^2/µm^3]	0.58	0.32	0.50
YSZ/Ni interface area [µm^2/µm^3]	0.86	0.58	0.79

Numerical results

Microstructural parameters of the simulated 3D geometries were computed every 500000 iterations and their time evolution is illustrated in Figure 2.

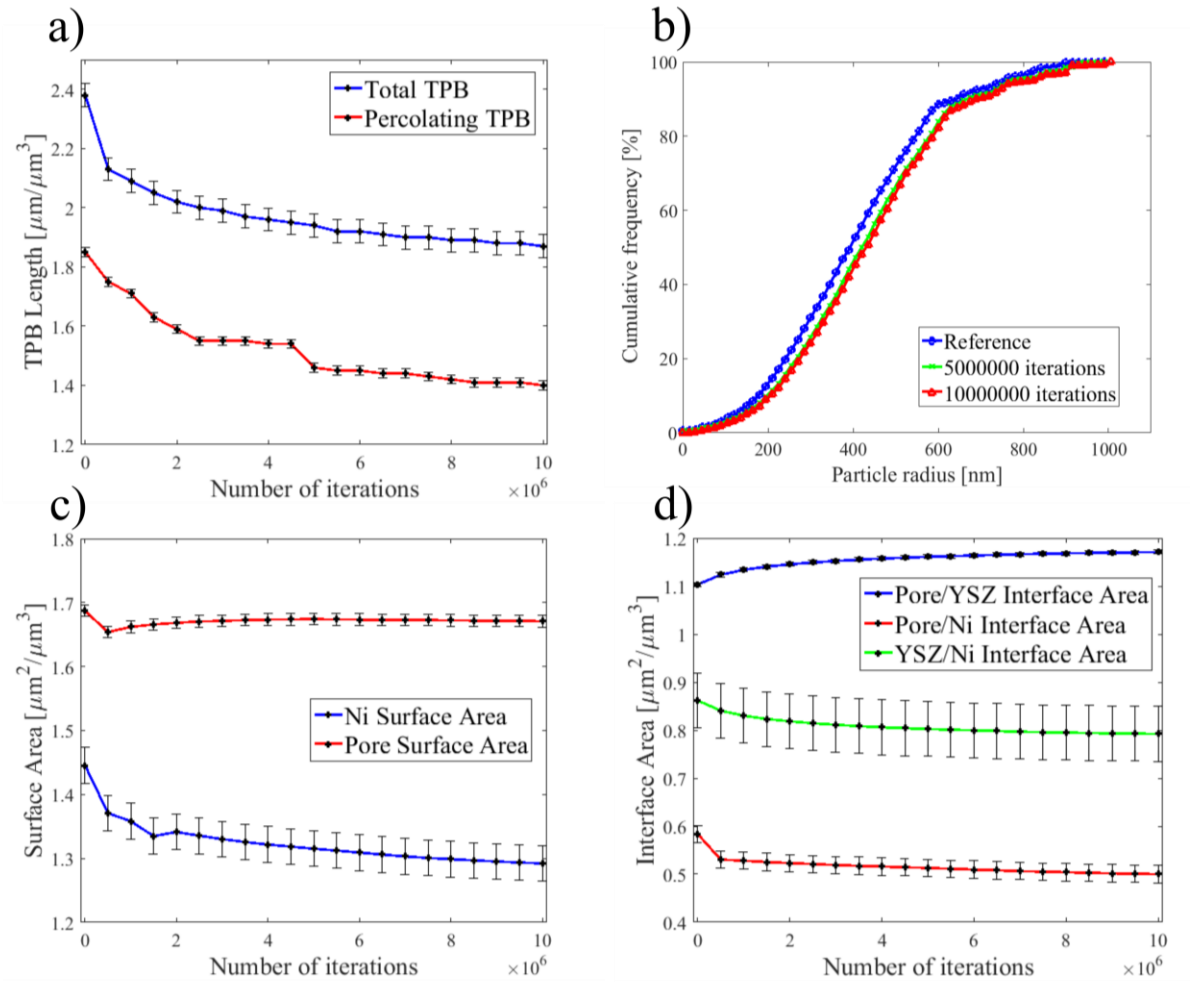

Figure 2. a) total and percolated TPB. b) continuous nickel PSD of the reference cell and two simulated geometries: 5 x 10^6 and 10^7 iterations. c) Ni and pores surface areas. d) Pore/YSZ, Pore/Ni and YSZ/Ni interface areas.

Figure 2a) shows a decrease of total and percolated TPB with time. The loss of active TPB length is faster in the first stages of the simulations while decreases at a slower rate after the first 2 million iterations, reaching a value of 1.40 μm/μm^3 after 10^7 iterations. The final values for total and percolated TPB length for the simulated volume are given in Table 2.

The Ni particle size distribution was computed after 5 x 10^6 iterations and at the end of the simulation, as shown in Figure 2b). A slight shift towards bigger Ni particles can be appreciated and ~ 50% of Ni particles have radii smaller than 450 nm after 10^7 iterations. In agreement with the results related to the TPBs, bigger changes are observed in the early steps of the simulation.

Figure 2c) and d) shows the trend of surface areas over time. Since we assume that, the YSZ is stable during the simulation, only Ni and pore surface areas change over time (Figure 2c)). The expected decreasing trend for overall Ni, YSZ/Ni, and pore/Ni interface area is observed. On the other hand, a slight increase in pore/YSZ interface area is observed. The values reached at the end of the simulation are presented in Table 2.

Furthermore, the phase fractions of Ni, YSZ, and pores were unvaried at the end of the computation, corresponding to 183 hours of operation, in the analyzed volume. This result is a proof that the mass in the computational domain is conserved in the model.

DISCUSSION

Figure 3a) and b) shows a 2D slice extracted from the reference and the last 3D simulated volume, respectively.

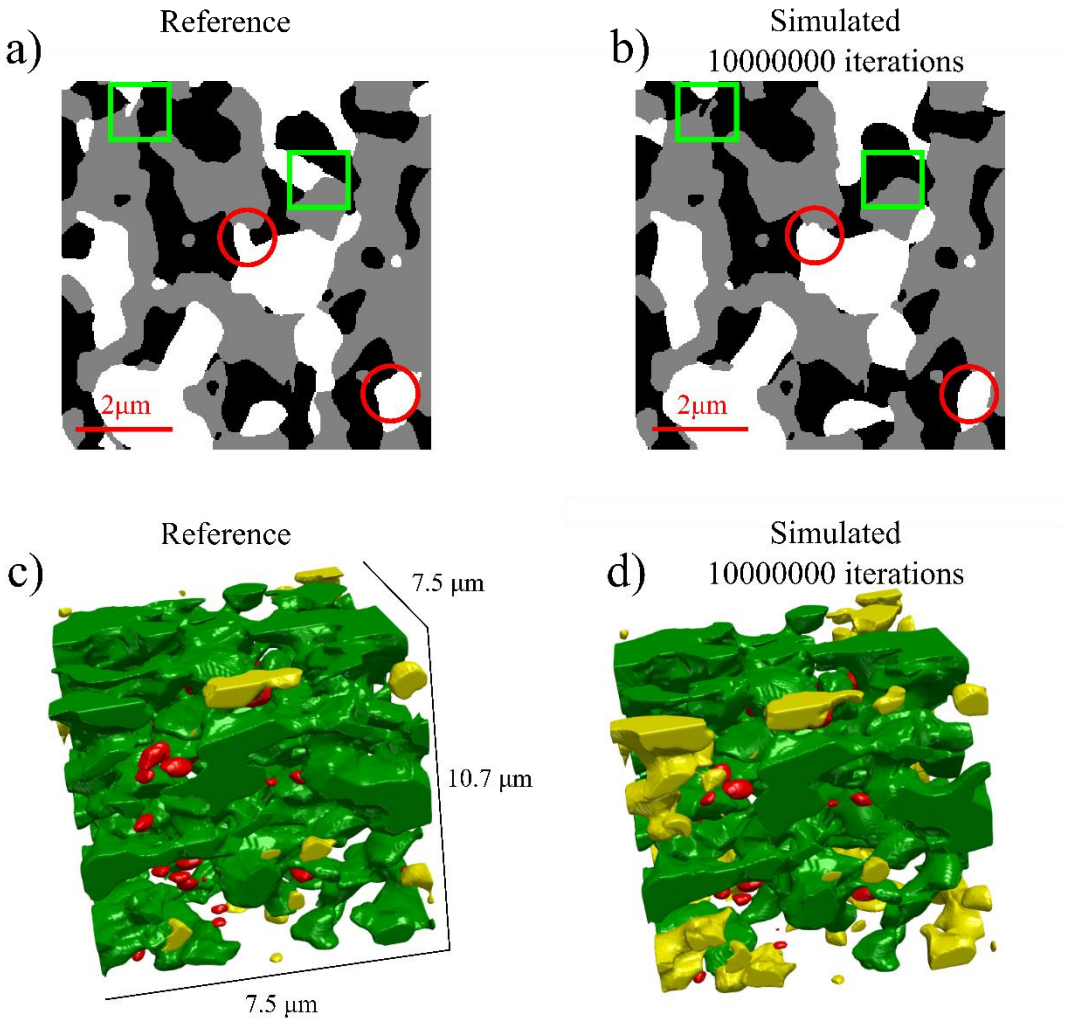

Figure 3. a) a two-dimensional slice from the three-dimensional volume of the reference cell. b) a two-dimensional slice from the three-dimensional volume of the simulated geometry after 10^7 iterations. c) a three-dimensional rendering of the Ni network in the reference cell. d) a three-dimensional rendering of the Ni network in the simulated geometry after 10^7 iterations. In a) and b) Ni is shown in white, YSZ is gray and pores are black. In c) and d) isolated Ni particles are red, connected Ni is green and Ni with unknown connectivity is yellow.

Microstructural changes in the Ni phase after 10^7 iterations can be observed in Figure 3b) compared to the reference cell (Figure 3a)). Since it is difficult to point out differences from complex 3D renderings, we base our discussion on the 2D slices presented in Figure 3a) and 3b). It is worth mentioning that, the phenomena present in this single slice are detected throughout the entire electrode. Two main phenomena can be identified: i) curvature minimization ii) nickel detachment from the YSZ network (nickel de-wetting).

The curvature minimization is observed in many locations inside the electrode and examples can be found in Figure 3b). Regions with high curvature, as those highlighted by the red circles in Figure 3a), evolve towards features having smoother interfaces. As a consequence of the curvature reduction, small protrusions present in the nickel network (as the ones highlighted by the red circles in Figure 3a)) disappear over time. This effect leads to the observed reduction in the overall Ni surface area. Furthermore, this effect contributes to the shift in the continuous PSD reported in Figure 2b).

Nickel de-wetting is highlighted by the green squares in Figure 3b). The detachment of nickel from the YSZ matrix leads to the creation of new pore/YSZ interfaces. This effect causes a decrease in Ni/YSZ interface area and a consequent slight increase in pore/YSZ interface area. This trend is reported in Figure 2d) and Table 2: Ni/YSZ interface area decreases from 0.86 $\mu m^2/\mu m^3$ to 0.79 $\mu m^2/\mu m^3$ at the end of the simulation and pore/YSZ interface subsequently increases from 1.10 $\mu m^2/\mu m^3$ to 1.17 $\mu m^2/\mu m^3$. Moreover, due to the de-wetting, TPB sites originally present in the reference cell disappear and the overall TPB length is reduced. This phenomenon contributes to explain the trend of the total TPB length observed in Figure 2a).

In order to explain the decrease of percolated TPBs, a connectivity study for the nickel network is performed. The comparison between the nickel connectivity in the reference cell and after 10^7 iterations is shown in Figure 3c) and d). The nickel network presents a decrease in connected nickel from 96.2 % in the reference cell to 75 % in the simulated volumes. The loss in connectivity in the modelling results is mainly due to the enlargement of regions where the connectivity of the nickel network is unknown (i.e. regions which appear isolated but might be connected outside the analyzed volume). This effect can be explained by the disconnection of the network inside the investigated volume and leads to the decrease of percolated TPB length observed in Figure 2a). With regard to the experimental data of the 9000 hours tested cell, the nickel loss in the innermost part of the fuel electrode has to be considered. The results reported in Table 2 show a decrease in nickel by ~ 14 % after the long-term operation. This effect contributes to the decrease of percolated TPBs in the tested cell. It is not taken into account in the modelling (at the present stage of refinement) and hence the loss of TPB is expected to be weaker in the model than in reality.

Based on the simulation results, we speculate that nickel undergoes a faster coarsening at the beginning of the operation. At this point, many nickel features with high curvature are still present in the Ni/YSZ cermet. As the coarsening progresses, the curvature of nickel particles decreases, decreasing the driving force for the nickel coarsening and thus the coarsening rate.

Besides the simulation results presented in this work, a complete model validation is required. Moreover, the operation conditions of the cell analyzed in this work (i.e. gas composition and polarization) are not considered in the PF model developed. In this regard, valuable data sets for the model validation can be obtained through ex-situ and in-situ x-ray tomography. In-situ or ex-situ X-ray tomography allows observation of the evolution of the same microstructural feature over time, and different atmospheres can be used for the experiments[30]. Finally, we can conclude that the model presented in this work can represent a valuable complementary tool to experimental characterization. While FIB-SEM tomography can be used to investigate statistically the microstructure evolution of long-term tested cell, PF modelling is able to simulate the evolution of the same microstructure. This ability allows obtaining time-resolved information of the microstructural changes, giving hints on the kinetics of the phenomena. Furthermore, having access to the evolution of the same features, hypothesis can be formulated on which part of the microstructure is less prone to the degradation. Therefore, a reliable PF model of SOC microstructure can represent a valuable tool in the ambitious aim of designing the microstructure of future electrodes with minimized degradation.

Error Analysis

For the statistical analysis of the experimental data, several error sources can affect the presented results. The 3D reconstructions obtained from FIB-SEM tomography can be influenced by changes in image quality. Furthermore, un-infiltrated pores can generate artifacts in the segmentation of the images. These segmentation errors cannot be avoided using the approach for processing the data presented in this work. In addition, the inhomogeneity of the volumes and

the intrinsic destructive nature of FIB-SEM tomography does not allow continuous tracking of the microstructure evolution. Moreover, the limited size of the sample analyzed may prevent fair representation of the full structure.

For the PF modelling, the assumptions made in order to simplify the model influence its reliability. In particular, the crystal orientations together with possible anisotropies of the atomic mobility and the polarization of the cell have a significant role in the microstructure evolution. Moreover, the use of a diffusive interface of a finite thickness limits the resolution of features smaller than the chosen interface width. Therefore, the evolution of such features cannot be resolved by the model and, in some cases, the limited resolution creates artifacts in the simulation results.

More modelling work is underway to: A) extend the calculations to longer times, B) validate further the behavior of the model by conducting a sensitivity study on the effects of the model parameters and further comparison to experiments, and finally C) introduce the effects of gradients in gas-composition to simulate the situation under operation.

CONCLUSIONS

The microstructural degradation of a Ni/YSZ electrode was investigated through FIB-SEM tomography and PF modelling. Statistical parameters were used to quantify changes in the microstructure with a focus on Ni coarsening.

Microstructural parameters were calculated on the reconstructed volumes of the reference and the tested cell, reconstructed through FIB-SEM tomography. A decrease in percolated TPB length was observed together with the loss of overall Ni surface area and Ni/YSZ interface area.

A PF model was developed to simulate nickel coarsening applying the reference cell microstructure as starting point. The results of the simulations show a decrease in Ni surface area, TPB length, and Ni/YSZ area. Furthermore, numerical results reveal that the coarsening is faster in the early stages of the simulation, showing that the coarsening proceeds at a slower rate after 2 millions of iterations. In the statistical analysis, error sources can arise from inaccuracies of the segmentation and the limited volume size. Furthermore, the reliability of the simulations can be affected by the limited resolution, due to the use of a diffuse interface.

Finally, PF modelling is illustrated to be a valuable complementary tool to experimental characterization. Once fully validated it is expected to provide design guide lines to structures that are less prone to degradation.

ACKNOWLEDGEMENTS

This work was financially supported by the project “Synfuel” (4106-00006B) from the Innovation Fund Denmark. The PF code and the 3D visualization of the results were realized thanks to the financial support of the “the alliance for ImagiNg of Energy Materials”, DSF-grant no. 1305-0032B via “The Danish Council for Strategic Research”. Moreover, the authors would like to thank senior researcher Jacob R. Bowen and staff at Haldor Topsøe A/S for their technical support.

REFERENCES

[1] Ebbesen S. D., Graves C., Hauch A., Jensen S. H., & Mogensen M. (2010). Poisoning of Solid Oxide Electrolysis Cells by Impurities Poisoning of Solid Oxide Electrolysis Cells by Impurities. *J. Electrochem. Soc., Volume 157 (10), B1419-B1429*.

[2] Fu Q., Mabilat C., Zahid M., Brisse A., & Gauiter L. (2010). Syngas production via high-temperature steam/CO_2 co-electrolysis: an economic assessment. *Energy & Environmental Science, Volume 3 (10), 1365-1608.*
[3] Laguna-Bercero M. A. (2012). Recent advances in high temperature electrolysis using solid oxide fuel cells: A review. *J. Power Sources, Volume 203, 4-16*.
[4] Hauch A., Ebbesen S. D., Jensen S. H., & M. Mogensen (2008). Solid Oxide Electrolysis Cells : Microstructure and Degradation of the Ni / Yttria-Stabilized Zirconia Electrode. *J. Electrochem. Soc., Volume 155 (11), B1184-B1193*.
[5] Knibbe R., Traulsen M. L., Hauch A., Ebbesen S. D., & Mogensen M. (2010). Solid Oxide Electrolysis Cells : Degradation at High Current Densities. *J. Electrochem. Soc., Volume 157 (8), B1209-B1217*.
[6] Tietz F., Sebold D., Brisse A., & Schefold J. (2013). Degradation phenomena in a solid oxide electrolysis cell after 9000 h of operation. *J. Power Sources, Volume 223, 129–135*.
[7] Chen M., Liu Y.-L., Bentzen J. J., Zhang W., Sun X., Hauch A., Tao Y., Bowen J. R., & Hendriksen P. V. (2013). Microstructural Degradation of Ni / YSZ Electrodes in Solid Oxide Electrolysis Cells under High Current. *J. Electrochem. Soc., Volume 160 (8), F883-F891.*
[8] Hauch A., Brodersen K., Chen M., & Mogensen M. B. (2016). Ni / YSZ electrodes structures optimized for increased electrolysis performance and durability. *Solid State Ionics, Volume 293, 27–36*.
[9] Holzer L., Iwanschitz B., Hocker Th., Münch B., Prestat M., Wiedenmann D., Vogt U., Holtappels P., Sfeir J., Mai A., & Graule Th. (2011). Microstructure degradation of cermet anodes for solid oxide fuel cells : Quantification of nickel grain growth in dry and in humid atmospheres. *J. Power Sources, Volume 196, 1279–1294*.
[10] Faes A., Hessles-Wyser A., Presvytes D., Vayenas C.G., & Vanherle J. (2009). Nickel – Zirconia Anode Degradation and Triple Phase Boundary Quantification from Microstructural Analysis. *Fuel Cells, Volume 9, 841-851.*
[11] Nakajo, A., Tanasini, P., Diethelm, S., Van herle, J. & Favrat, D. (2011). Electrochemical Model of Solid Oxide Fuel Cell for Simulation at the Stack Scale II: Implementation of Degradation Processes. *J. Electrochem. Soc. 158, B1102-B118*.
[12] Chen H. Y., Yu H. C., Cronin J. S., Wilson J. R., Barnett S. A., & Thonrnton K. (2011). Simulation of coarsening in three-phase solid oxide fuel cell anodes. *J. Power Sources, Volume 196, 1333–1337*.
[13] Vaßen R. Simwonis D., & Stöver D., (2001). Modelling of the agglomeration of Ni-particles in anodes of solid oxide fuel cells. *J. Materials Science, Volume 36, 147–151.*
[14] Mogensen M. B., Hauch A., Sun X., Chen M., Tao Y., Ebbesen S. D., Hansen K. V., & Hendriksen P. V. (2017). Relation Between Ni Particle Shape Change and Ni Migration in Ni – YSZ Electrodes – a Hypothesis. *Fuel Cells, Volume 17, 434-441.*
[15] Trini M. Jørgensen P. S., Hauch A., Chen M., & Hendriksen P. V. (2017). Microstructural Characterization of Ni/YSZ Electrodes in a Solid Oxide Electrolysis Stack Tested for 9000 Hours. *ECS Transactions, Volume 78 (1), 3049-3064*.
[16] Gao S., Li J. & Lin Z. (2014). Theoretical model for surface diffusion driven Ni-particle agglomeration in anode of solid oxide fuel cell. *J. Power Sources, Volume 255, 144–150* .
[17] Kennouche D., Chen-Wiegart Y. K., Riscoe C., Wang J., & Barnett S. A. (2016). Combined electrochemical and X-ray tomography study of the high temperature evolution of Nickel – Yttria Stabilized Zirconia solid oxide fuel cell anodes. *J. Power Sources, Volume* ***307,*** *604–612.*
[18] Jiao Z., & Shikazono N. (2014). Simulation of Nickel Morphological and Crystal Structures Evolution in Solid Oxide Fuel Cell Anode Using Phase Field Method. *J. Electrochem. Soc., Volume 161, F577–F582*.

[19] Lei Y., Cheng T. & Wen Y. (2017). Phase field modeling of microstructure evolution and concomitant effective conductivity change in solid oxide fuel cell electrodes. *J. Power Sources, Volume 345, 275–289*.
[20] Chen L. (2002). PHASE -FIELD MODELS FOR MICROSTRUCTURE. Annu. Rev. Mater Res. 2002. DOI:10.1146/annurev.matsci.32.112001.132041.
[21] Brisse A., Schefold J., Corre G., & Fu Q. (2014). Performance and Lifetime of Solid Oxide Electrolyzer Cells and Stacks. *11th European SOFC & SOEC Forum, B1405, 48–59*.
[22] Jørgensen P. S., Ebbehøj S. L., & Hauch A. (2015). Triple phase boundary specific pathway analysis for quantitative characterization of solid oxide cell electrode microstructure. *J. Power Sources, Volume 279, 686–693*.
[23] Münch B., & Holzer L. (2008). Contradicting Geometrical Concepts in Pore Size Analysis Attained with Electron Microscopy and Mercury Intrusion. *J. Am. Ceram. Soc., Volume 91, 4059-4067.*
[24] Knibbe R., Hauch A., Hjelm J., Ebbesen S. D. & Mogensen M. (2011). Durability of Solid Oxide Cells. *Green, Volume 1, 141–169*.
[25] Blakely J. M., & Mykura H. (1961). The Effect of Impurity Adsorption on the Surface Energy and Surface Self Diffusion in Nickel. *Acta Metallurgica, Volume 9, 595-599*.
[26] Chen H. Y., Yu H. C., Cronin J. S., Wilson J. R., Barnett S. A., & Thornton K. (2012). Ni coarsening in the three-phase solid oxide fuel cell anode – a phase-field simulation study. arXiv:1201.1567 [physics.comp-ph]
[27] Yu H., Chen H., & Thornton K. (2012). Extended smoothed boundary method for solving partial differential equations with general boundary. *Modelling Simul. Mater. Sci. Eng., Volume 20, 75008*.
[28] Abdullah T., & Liu L. (2016). Meso-Scale Phase-Field Modeling of Microstructural Evolution in Solid Oxide Fuel Cells. *J. Electrochem. Soc., Volume 163 (7), F618-F625*.
[29] Davis R., Abdeljawad F., Lillibridge J., & Haataja M. (2014). ScienceDirect Phase wettability and microstructural evolution in solid oxide fuel cell anode materials. *Acta Mater. Volume 78, 271–281*.
[30] De Angelis S., Jørgensen P. S., Esposito V., Tsai E. H. R., Holler M., Kreka K., Abdellahi E., & Bowen J. R. (2017) Ex-situ tracking solid oxide cell electrode microstructural evolution in a redox cycle by high resolution ptychographic nanotomography. *J. Power Sources, Volume 360, 520–527*.